Article

The Receptor for Hyaluronan-Mediated Motility (CD168) promotes inflammation and fibrosis after acute lung injury

Zheng Cui[a,†], **Jie Liao**[b,†], **Naeun Cheong**[b,†], **Christopher Longoria**[b], **Gaoyuan Cao**[c], **Horace M. DeLisser**[c] **and Rashmin C. Savani**[a,b,d]

a - Division of Neonatology, *Children's Hospital of Philadelphia, University of Pennsylvania School of Medicine, Philadelphia, PA, USA*
b - Center for Pulmonary & Vascular Biology, *Department of Pediatrics, University of Texas Southwestern Medical Center, Dallas, TX, USA*
c - Perelmen Center for Advanced Medicine, *Department of Medicine, University of Pennsylvania School of Medicine, Philadelphia, PA, USA*
d - Division of Neonatal-Perinatal Medicine, *Department of Pediatrics, University of Texas Southwestern Medical Center, Dallas, TX, USA*

Correspondence to Rashmin C. Savani: *Center for Pulmonary & Vascular Biology, Division of Neonatal-Perinatal Medicine, University of Texas Southwestern Medical Center, 5323 Harry Hines Boulevard, Dallas, TX 75390-9063, USA.*
rashmin.savani@utsouthwestern.edu
https://doi.org/10.1016/j.matbio.2018.08.002

Abstract

Acute lung injury results in early inflammation and respiratory distress, and later fibrosis. The glycosaminoglycan hyaluronan (HA) and the Receptor for Hyaluronan-Mediated Motility (RHAMM, CD168) have been implicated in the response to acute lung injury. We hypothesized that, compared to wild type (WT) mice, RHAMM knockout (KO) mice would be protected from, whereas mice with macrophage-specific transgenic overexpression of RHAMM (TG) would have worse inflammation, respiratory distress and fibrosis after intratracheal (IT) bleomycin. Compared to WT mice, 10 days after IT bleomycin, RHAMM KO mice had less weight loss, less increase in respiratory rate, and fewer CD45+ cells in the lung. At day 28, compared to injured WT animals, injured RHAMM KO mice had lower M1 macrophage content, as well as decreased fibrosis as determined by trichrome staining, Ashcroft scores and lung HPO content. Four lines of transgenic mice with selective overexpression of RHAMM in macrophages were generated using the Scavenger Receptor A promoter driving a myc-tagged full length RHAMM cDNA. Baseline expression of RHAMM and CD44 was the same in WT and TG mice. By flow cytometry, TG bone marrow-derived macrophages (BMDM) had increased cell surface RHAMM and myc, but equal CD44 expression. TG BMDM also had 2-fold increases in both chemotaxis to HA and proliferation in fetal bovine serum. In TG mice, increased inflammation after thioglycollate-induced peritonitis was restricted to macrophages and not neutrophils. For lung injury studies, non-transgenic mice given bleomycin had respiratory distress with increased respiratory rates from day 7 to 21. However, TG mice had higher respiratory rates from 4 days after bleomycin and continued to increase respiratory rates up to day 21. At 21 days after IT bleomycin, TG mice had increased lung macrophage accumulation. Lavage HA concentrations were 6-fold higher in injured WT mice, but 30-fold higher in injured TG mice. At 21 days after IT bleomycin, WT mice had developed fibrosis, but TG mice showed exaggerated fibrosis with increased Ashcroft scores and HPO content. We conclude that RHAMM is a critical component of the inflammatory response, respiratory distress and fibrosis after acute lung injury. We speculate that RHAMM is a potential therapeutic target to limit the consequences of acute lung injury.

Introduction

Acute lung injury is characterized by an initial inflammatory response that coincides with acute respiratory distress and surfactant deficiency, and which precedes a more chronic pulmonary fibrosis [1–3]. The prevailing model of acute lung injury is that injury to the epithelium results in the release of inflammatory mediators, promoting the influx initially of neutrophils and subsequently macrophages into sites of injury, with further increases in cytokine production and modulation of the extracellular matrix, including fibronectin, elastin, hyaluronan, and collagen [4–7]. Hyaluronan (hyaluronic acid, HA) is a non-sulfated glycosaminoglycan that consists of a polymer of repeating disaccharide units of *N*-acetyl glucosamine and glucuronic acid [8,9]. Increased recovery of HA has been demonstrated in bronchoalveolar lavage (BAL) from human inflammatory and fibrotic lung diseases such as sarcoidosis [10], occupational lung disorders [11], and ARDS [12]. The accumulation of inflammatory cells at sites of injury requires their activation, adhesion to endothelium, and subsequent transmigration into the injured tissue. Although the precise role that HA plays in these processes is not clear, HA has been implicated in tissue responses to injury. Thus, HA is involved in monocyte activation [13], in leukocyte adhesion to endothelium [14–16], and in smooth-muscle cell migration after wounding [17]. Interestingly, HA-binding peptides inhibit macrophage motility in vitro [18] and, when administered in vivo, reduce inflammation and fibrosis during skin wound repair [19], in a dinitrofluorobenzene (DNFB) model of cutaneous inflammation [20], in ozone-induced airway hyperresponsiveness [21], and after acute lung injury [18]. These data suggest that HA is upstream of and contributes to the inflammatory response to tissue injury.

HA modifies cell behavior through interactions with at least two molecularly distinct cell-associated receptors, CD44 and Receptor for HA-Mediated Motility (RHAMM, CD168), and both have been implicated in acute lung injury [22]. Thus, CD44 expression is increased after bleomycin injury [23,24], and acute lung injury in CD44 knockout mice results in the accumulation of inflammatory cells and excess HA accumulation, suggesting that CD44 is necessary for the resolution of inflammation [25]. RHAMM is expressed at the cell surface, in the cytoplasm and in the nucleus, and regulates cell locomotion and proliferation [17,26,27]. In several injury models, RHAMM and HA are overexpressed in macrophages [28], fibroblasts [29], epithelial cells [30], and smooth muscle cells [17] responding to injury. Our previous studies, in a rat intratracheal bleomycin model of acute lung injury and fibrosis, showed that RHAMM and HA expression are increased in macrophages responding to injury, and that the increased motility of these cells was entirely dependent on RHAMM and HA [18,31]. Interestingly, both HA-binding peptide and antibody blockade of RHAMM in vivo decreased the accumulation of macrophages into the bleomycin-injured lung, suggesting that RHAMM-HA interactions are crucial for the recruitment of these cells to the site of injury [18,31]. However, these studies did not define the particular cell type that contributed to the overall findings, did not determine macrophage-specific functions of RHAMM, and the antibody inhibition studies required confirmation using genetically-modified mouse models. Therefore, using the IT bleomycin model of acute lung injury, we conducted loss of function studies using RHAMM knockout mice, and gain of function studies using transgenic mice with overexpression of RHAMM specifically in macrophages. We here demonstrate that bleomycin-injured RHAMM KO mice had less weight loss and respiratory distress, less accumulation of macrophages and HA, and less fibrosis after IT bleomycin than WT mice. Transgenic overexpression of RHAMM in macrophages resulted in increased transgene expression on the cell surface, and increased macrophage chemotaxis and proliferation. Interestingly, thioglycollate-induced peritonitis in TG mice specifically exaggerated macrophage and not neutrophil infiltration, suggesting that RHAMM was driving cell-specific effects in transgenic mice. Bleomycin injury in TG mice resulted in worse inflammation and respiratory distress, increased HA accumulation and worse fibrosis than in WT animals. Collectively, these data demonstrate that RHAMM is a critical component of the recruitment of macrophages and subsequent fibrosis after acute lung injury.

Results

RHAMM KO mice are protected from bleomycin-induced respiratory distress and inflammation

Given the sex differences in bleomycin-induced lung injury in mice, with males having worse outcomes than females [32], only male mice were used in all experiments. For all measurements, unmanipulated mice and mice given intratracheal saline as controls did not differ and these groups were therefore combined as a single control group. The percent change in weight from the start of the experiment was used as a surrogate for the severity of illness in mice given either intratracheal bleomycin or an equivalent volume of sterile saline as a control. Both control groups of WT and KO mice gained weight steadily over the 28-day duration of the experiment (Fig. 1a). WT mice given IT bleomycin lost approximately 15% body weight over the first 10 days, and then regained weight by 28 days. In contrast, RHAMM KO mice lost only 7% body weight over the first 10 days and then regained weight by 28 days (Fig. 1a).

In order to measure the degree of respiratory distress after acute lung injury, the respiratory rates of non-sedated mice were determined using dual chamber plethysmography. All mice had similar baseline respiratory rates (data not shown). The percent change from baseline was determined at 4, 7, 10, 14, 21 and 28 days after IT treatments. Control mice showed no changes in respiratory rates for the duration of the experiment (Fig. 1b). WT mice given IT bleomycin had between 20% increase on day 4 to a maximum of 35% increase in respiratory rates on day 10 after injury. Respiratory rates in injured WT mice then decreased but remained elevated from baseline until day 28 (Fig. 1b). RHAMM KO mice, however, had a maximum 20% increase in respiratory rate at 10 days after injury (Fig. 1b), suggesting less respiratory distress in the absence of RHAMM.

Since we have previously shown that the respiratory distress observed after bleomycin injury is associated with the early inflammatory response and not the fibrotic sequela [33], we next examined lung inflammation. Flow cytometry studies of the lung on day 10 after IT bleomycin showed that WT mice had increased accumulation of CD45+ cells expressed both as percent of total live cells and as absolute numbers (Fig. 1c). In addition, the *N*-acetyl glucosaminidase (NAG) activity of cells obtained by BAL, a measure of M1 macrophages [34], was determined using an established assay [35]. On day 28 after injury, when WT mice had a substantial 10-fold increase in NAG activity in BAL cells, RHAMM KO mice had a significantly lower 2-fold increase in NAG activity ($P < 0.001$ vs. WT bleomycin, Fig. 1d). We and others have correlated elevated lung HA content with an acute inflammatory response after injury [18,36–38]. We therefore measured the HA content of BAL in WT and RHAMM KO mice (Fig. 1e). Bleomycin injury was associated with a 40-fold increase in HA content of BAL in WT mice. On the other hand, RHAMM KO mice had a lower, 10-fold increase in HA content with the same degree of bleomycin injury (Fig. 1e). We also localized HA using a biotinylated fragment of aggrecan as a HA-binding probe (bHABP) in affinity histochemistry (Fig. 1f). Wild type control and IT saline-treated mice had the expected distribution of HA around bronchiolar smooth muscle and in the adventitial layer of blood vessels, with little to no staining in the peripheral lung. RHAMM KO mice had a similar baseline HA distribution to WT mice (Fig. 1f). In WT mice ten days after IT bleomycin injury, increased HA staining was observed, in particular in the peripheral lung parenchyma (Fig. 1f). However, this increase in peripheral HA localization was not seen in RHAMM KO mice (Fig. 1f).

RHAMM KO mice have less fibrosis after intratracheal bleomycin-induced lung injury

We next determined the degree of fibrosis in WT and RHAMM KO mice at 28 days after IT treatments. First, we used trichrome staining of sections of lungs obtained from WT and RHAMM KO mice after either IT saline or bleomycin treatment to evaluate fibrosis histologically. Compared to saline-treated animals, bleomycin-injured WT mice had patchy areas of fibrosis, atelectasis and over-distension (Fig. 2a). Bleomycin-injured RHAMM KO mice, on the other hand, had more normal distal lung architecture, with distinctly fewer areas of fibrosis, atelectasis and over-distension (Fig. 2a). Histologic samples were quantified by two independent and blinded observers to determine Ashcroft score [39]. WT mice showed an eight-fold increase in Aschcroft score with bleomycin injury (Fig. 2b). RHAMM KO mice, on the other hand, had only a three-fold increase in Ashcroft score (Fig. 2b). In order to biochemically quantify fibrosis, we determined the hydroxyproline (HPO) content of WT and KO lungs after saline or bleomycin treatments. Lungs from WT mice injured with bleomycin had a two-fold higher HPO content than WT saline-treated animals (Fig. 2c). However, the lungs of bleomycin-treated RHAMM KO mice had HPO contents that were similar to uninjured or saline-treated WT mice (Fig. 2c).

Collectively, these data show that, in WT mice, the early phase of acute lung injury is associated with severe weight loss, respiratory distress, increased lung HA content, and macrophage accumulation. The bleomycin-injured lung of WT mice then undergoes a chronic fibrotic change. Targeted deletion of RHAMM is associated with less weight loss and respiratory distress, lower lung HA content, and decreased macrophage accumulation. Additionally, at later time points of the model, RHAMM KO mice are protected from bleomycin-induced lung fibrosis.

Generation of mice with transgenic overexpression of RHAMM in macrophages

A transgenic construct consisting of 5 kb of the Scavenger Receptor A (SRA) promoter driving a myc-tagged full length 2.4 kb RHAMM cDNA was generated as described in Methods (Fig. 3a). The transgenic facility at the University of Pennsylvania injected 150 fertilized eggs with this transgenic construct and generated 38 C57/Bl6-129 mice. Genotyping of these mice was accomplished by Southern blotting of genomic DNA using a 4.5 kb fragment of the transgene generated using the restriction enzyme *Nsi1*. Four independent transgene positive mice with varying copy numbers were identified (SRA8, 2 copies; SRA15, 1 copy, SRA22, 2 copies and SRA27, 10 copies, Supplementary Fig. 1a and b). Each transgenic line was backcrossed to pure C57/Bl6J background for greater than nine generations. Bone marrow-derived macrophages (BMDM) were obtained from WT C57/Bl6 and each of the transgenic lines. The steady state content of transgenic mRNA in these cells was determined

using RT-PCR with primers that spanned from the myc tag to RHAMM and generated a 750 bp product (Supplementary Fig. 1c). RT-PCR of GAPDH was used as a control and generated a 360 bp fragment. While WT mice had a GAPDH product, they did not have the transgenic construct, whereas each of the transgenic lines had both GAPDH and transgenic DNA (Supplementary Fig. 1c). Western blot analysis of BMDM probed with myc antibody showed two bands at 93 kDa and 70 kDa with variable expression of each band in different transgenic lines (Supplementary Fig. 1d). The 93 kDa protein band represents full length RHAMM whereas we have previously associated the 70 kDa protein band with cell surface expression and motile responses [31].

In order to further characterize the RHAMM transgenic mice, we obtained BMDM from WT and each of the transgenic lines. Once fully differentiated into BMDM in vitro, the cells were examined by immunofluorescence with antibodies that detected

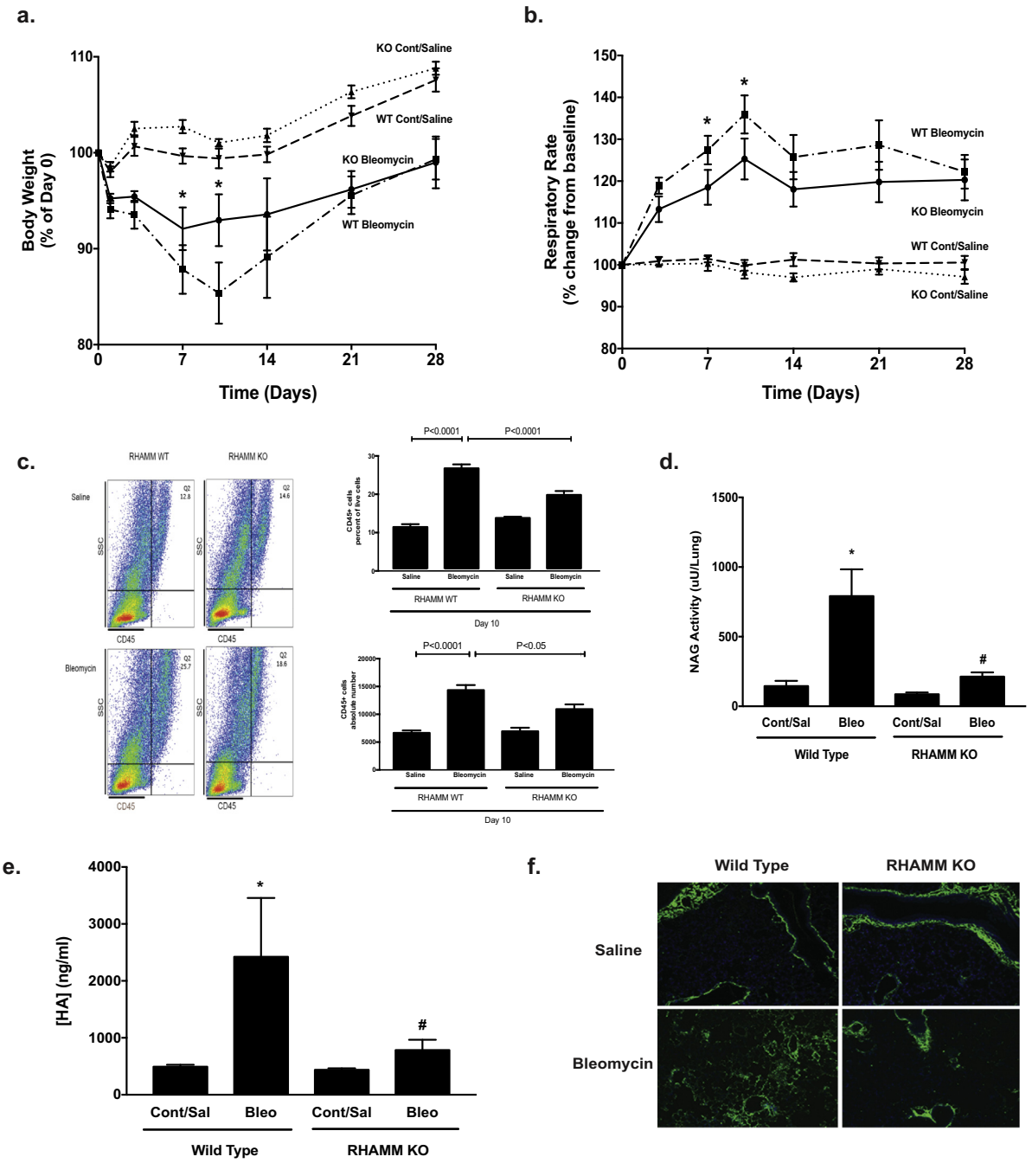

either the macrophage marker F4/80 or myc. Both WT and transgenic macrophages were recognized by F4/80 antibody (Fig. 3b). However, WT macrophages had a rounded appearance, whereas transgenic macrophages from each of the four transgenic lines had an elongated, spindle shape suggestive of more motile cells (Fig. 3b, data shown for SRA22). Since the appearance of these transgenic macrophages was similar to fibrocytes, we examined the expression of fibrocyte markers [40]. We first confirmed that the BMDM were CD45+, CD31– and CD34– (data not shown). We then examined the expression of Fibronectin, CD105 and Collagen I in WT and TG BMDM by quantitative RT-PCR. The expression of Fibronectin, CD105, and Collagen I were all low and were not influenced by expression of the transgene (Fig. 3c), suggesting that transgenic expression of RHAMM in macrophages did not drive a fibrocyte phenotype. Further, macrophages from each of the transgenic lines, but not WT C57/Bl6 macrophages, stained for myc, thereby confirming specific transgene expression (Fig. 3d). To determine cell surface expression of the transgene, flow cytometry was performed on BMDM using antibodies to myc, RHAMM and CD44 (Fig. 3e). WT macrophages had expression of RHAMM and CD44, but not myc. Transgenic macrophages showed increased expression of myc as well as RHAMM. Of note, there was equivalent CD44 expression on both WT and TG macrophages (Fig. 3e).

We next examined the effects of transgene expression on the chemotaxis of BMDM. Chemotaxis was examined to a six-dimer fragment of HA (HA6) and 10% FBS. Data were normalized as fold change over WT cells with defined medium in the lower chamber as a chemoattractant. Responses to FBS were variable between macrophages from each of the transgenic lines (Fig. 3f). A five-fold increase in chemotaxis to HA was seen in WT cells. However, a further 2–3-fold increase above this response was seen in transgenic cells, suggesting a specific effect of HA with the RHAMM transgene (Fig. 3f). To determine proliferation, BMDM were maintained in 1% FBS overnight and then exposed to fresh 10% FBS every 24 h. Cell numbers were normalized as fold change over WT macrophages at the start of the experiment. While WT BMDM did not show any appreciable proliferation, macrophages from each of the transgenic lines showed 2 to 3.5-fold increase in proliferation over 48 h (Fig. 3g).

In vivo effects of over-expression of RHAMM in macrophages

In order to determine the in vivo specificity of the transgene for macrophages, we employed the intraperitoneal (IP) thioglycollate model of peritonitis. In this model, thioglycollate elicits an initial neutrophil (24 h) followed by a macrophage (5 days) influx into the peritoneal cavity [41]. We therefore examined peritoneal inflammation after thioglycollate both at 24 and 72 h in WT and each of the four transgenic lines. At every time point examined, IP saline instillation did not elicit any inflammatory response. At 24 h after IP thioglycollate, WT and each transgenic line showed equivalent peritoneal infiltration of neutrophils (Fig. 4a). At 72 h after IP thioglycollate, WT mice had no appreciable macrophage accumulation in the peritoneal cavity. However, each transgenic mouse line showed 3–6-fold increase in peritoneal macrophage infiltration (Fig. 4a), suggesting that the effect of transgene expression in macrophages

Fig. 1. Bleomycin-induced acute lung injury in WT and RHAMM KO mice. (a). The change in body weight over time after IT treatments was used as a measure of severity of illness. Unmanipulated and IT saline-treated control mice showed weight gain over time. WT mice given IT bleomycin lost weight over the first 10 days with a maximum weight loss of 15%. These mice then gained weight thereafter and approached their starting weight by day 28. Bleomycin-injured RHAMM KO mice had less weight loss than WT mice on days 7 and 10, losing a maximum of 7% of starting body weight ($^{*}P < 0.01$ vs. WT bleomycin, n = 8–12 mice/group). (b). Using non-sedated, dual chamber plethysmography, the change in respiratory rate from baseline was determined in WT and RHAMM KO mice after IT treatments as a measure of respiratory distress. Unmanipulated and IT saline-treated control mice showed no changes in respiratory rates over time. WT mice given bleomycin had increased respiratory rates from day 4 onwards, with a maximum 35% increase on day 10, after which respiratory rates decreased, but never returned to baseline. RHAMM KO mice had lower respiratory rates on days 7 and 10 after IT bleomycin than WT mice, increased to a maximum of 20% on day 10 ($^{*}P < 0.05$ vs. WT bleomycin, n = 6 mice per group). (c). Flow cytometry of total lung cells showed a two-fold increase in CD45+ cells in WT mice 10 days after bleomycin injury measured both as percent of total cells and absolute cell numbers. RHAMM KO mice had lower 30% increase in CD45+ cells after IT bleomycin. (d). Content of M1 macrophages obtained by BAL on day 28 was determined using the NAG activity assay. Unmanipulated and saline-treated animals showed no inflammation. Bleomycin injury in WT mice resulted in a 10-fold increase in NAG activity over saline-treated controls ($^{*}P < 0.0001$, n = 8–12 mice). RHAMM KO mice given bleomycin had a lower 2-fold increase in NAG activity compared to bleomycin-injured WT mice ($^{\#}P < 0.001$, n = 8–12 mice). (e). The HA content of BAL was increased 40-fold in WT mice injured with IT bleomycin ($^{*}P < 0.0001$ vs. saline controls, n = 8–12 mice). Bleomycin-treated RHAMM KO mice a lower 10-fold increase in HA content compared to KO mice given saline, and substantially lower HA content as compared to WT mice given bleomycin ($^{\#}P < 0.001$, n = 8–12 mice). (f). In control WT mice, HA, localized using affinity histochemistry, was distributed around bronchiolar airway smooth muscle and in the adventitia or pulmonary blood vessels. Bleomycin injury in WT mice resulted in increased parenchymal staining for HA. Bleomycin injury in RHAMM KO mice was not associated with distal lung parenchymal staining for HA.

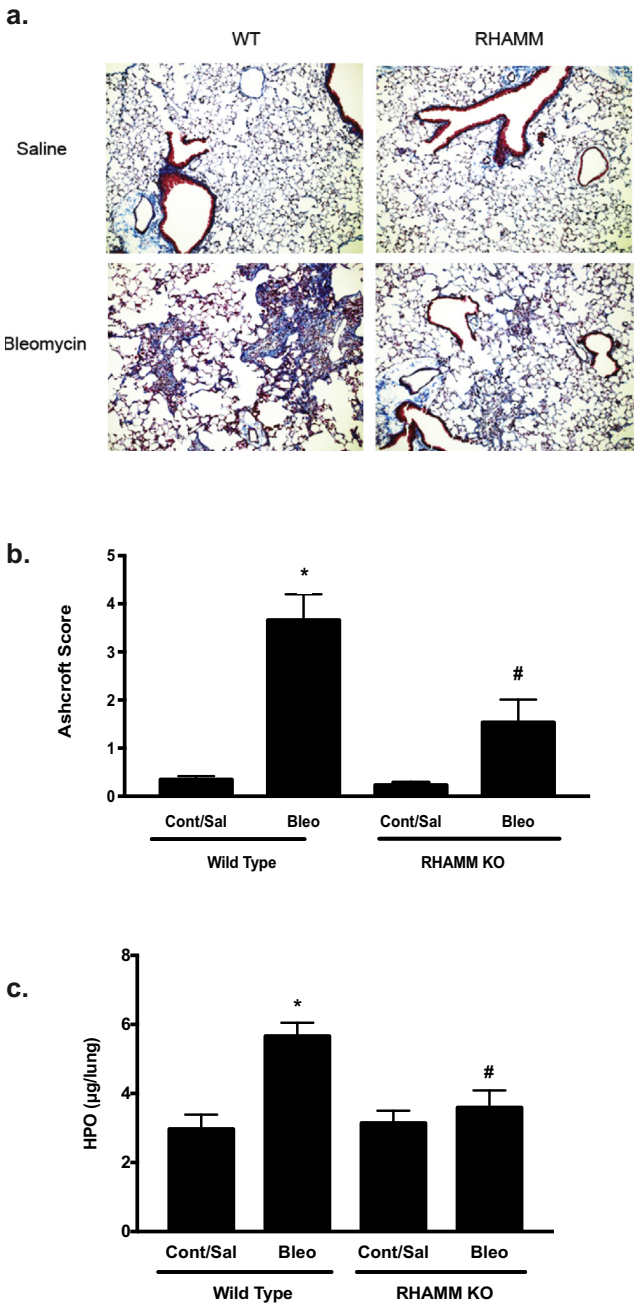

Fig. 2. Bleomycin-induced lung fibrosis in WT and RHAMM KO mice. (a). Fibrosis was assessed using Masson's trichrome staining of lung tissue sections at 28 days after treatments. WT mice given IT saline had normal lung architecture. After IT bleomycin, WT mice had patchy areas of cellular infiltrate, fibrosis, atelectasis and over-distension. Bleomycin-injured RHAMM KO mice had a more normal lung architecture with fewer areas of fibrosis. (b). Ashcroft score was used to quantify the degree of fibrosis. Compared to saline-treated controls, WT mice given IT bleomycin had 8-fold increased Ashcroft scores ($^{*}P < 0.001$ vs. WT saline, n = 4–6 mice). RHAMM KO mice given bleomycin had a lower 3-fold increase in Ashcroft scores ($^{\#}P < 0.001$ vs. WT bleomycin, n = 4–6 mice). (c). Lung hydroxyproline (HPO) content was determined to quantify fibrosis biochemically. WT mice given IT bleomycin had 2-fold increased HPO content ($^{*}P < 0.05$ vs. WT IT saline, n = 4–6 mice). Bleomycin-treated RHAMM KO mice did not show any increase in HPO content over KO mice given IT saline and had lower HPO content than WT mice given bleomycin ($^{\#}P < 0.05$ vs. WT IT bleomycin, n = 4–6 mice).

was an effect specific to the cell type and not an alteration of the environment to promote general inflammation.

We next studied IT bleomycin in macrophage RHAMM over-expressing mice, again using only male mice. In preliminary experiments, the IT dose of 1 U/kg used in WT/RHAMM KO experiments above was found to cause excessive mortality in TG mice (data not shown). We therefore used 0.5 U/kg IT to examine the effects in WT and TG mice. Again, unmanipulated and IT saline-treated mice were no different and these data were combined. We first examined respiratory rates as done previously for WT and RHAMM KO mice. After 0.5 U/kg IT bleomycin, WT mice had a 30% increase in respiratory rate between 7 and 14 days (Fig. 4b). We examined the same dose of IT bleomycin in the SRA8 and SRA22 lines. In contrast to WT mice, TG mice had 30% increased respiratory rates by 4 days and continued to worsen to a maximum of almost

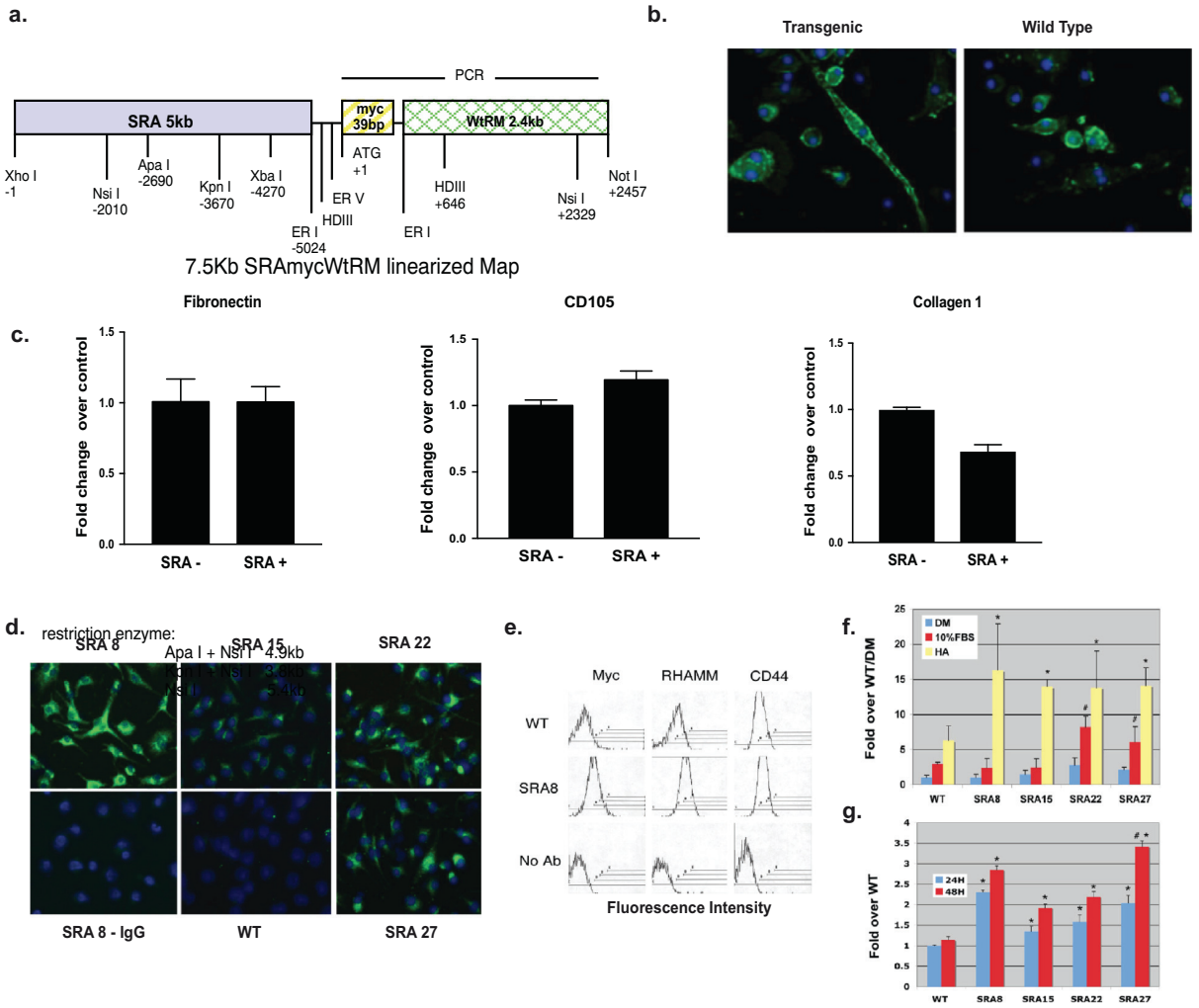

Fig. 3. Generation and characterization of transgenic mice overexpressing RHAMM in macrophages. (a). A transgenic construct, the product of *Xho1*/*Not1* restriction enzyme digestion and consisting of a 5 kb Scavenger Receptor A promoter driving a myc-tagged (39 bp) full length mouse RHAMM cDNA (2.4 kb), was generated as described in Methods. A 4.5 kb probe for use in Southern blots was generated by digestion with *Nsi1*. RT-PCR primers were designed to amplify myc-RHAMM to allow identification of the transgene. 150 fertilized eggs were injected yielding 38 mice, four of which were positive for the transgene. (b). BMDM were obtained from WT and TG mice and stained for the macrophage marker F4/80. WT macrophages retained their rounded appearance, whereas TG macrophages were long and spindle-shaped reminiscent of motile cells. (c). Expression of fibrocyte markers were determined in BMDM obtained from SRA- controls and TG positive mice. Expression of all markers was low and unaffected by RHAMM transgene expression. (d). Myc-tag antibody staining of BMDM in culture showed variable staining in each of the TG lines, but none in the C57/Bl6J cells. Normal IgG, used as a staining control, showed no staining in SRA8 cells. (e). Flow cytometry evaluation for surface expression of myc, RHAMM and CD44 on BMDM from WT and TG mice showed that TG mice had increased RHAMM and myc, but equivalent CD44 expression. (f). The chemotactic behavior of WT and TG BMDM was assessed using a Boyden chamber assay using HA6 as a chemoattractant (yellow bars), with defined medium (DM, blue bars) and 10% FBS (red bars) as negative and positive controls respectively. FBS elicited variable chemotactic responses in WT and each of the TG lines. WT macrophages showed a 5-fold increase in chemotaxis in response to HA6. Macrophages from each TG line had a further 2–3-fold increase above the WT response to HA6 ($^{*}P < 0.05$ vs. WT HA-treated cells, n = 5 wells per experiment, representative data from two independent experiments). (g). As expected for macrophages in culture, the cell numbers of WT macrophages did not change over 48 h. Each of the transgenic macrophages showed a 2–3.5-fold increase in cell numbers suggesting increased proliferation with transgene expression ($^{*}P < 0.01$ vs. WT controls at equivalent times and $^{\#}P < 0.05$ vs. SRA27 at 24 h, n = 5 wells per experiment, representative data from two independent experiments).

70% above baseline at 21 days when the experiment had to be terminated as the mice were moribund (Fig. 4b).

Lung inflammation was examined using flow cytometry in a single cell preparation of the lungs on day four after IT treatments (Fig. 4c). At this early time point, WT mice had not mounted an inflammatory response to IT bleomycin (Fig. 4c). However, TG mice had a two-fold increase in CD45+ cells in the lung compared to WT mice (Fig. 4c). The accumulation of M1 macrophages in lung lavage, as measured by the NAG activity of cell pellets obtained after BAL obtained on day 21 after injury, increased four-fold in WT mice given bleomycin (Fig. 4d). However, TG mice under the same conditions had a seven-fold increase in M1 macrophage influx after bleomycin (Fig. 4d). We also examined the lung content and distribution of HA in WT and TG mice. We determined the HA content of BAL at 21 days after treatments. While WT mice had a five-fold increase, TG mice had 20–25-fold increase in BAL HA content (Fig. 4e). Staining for HA in sections of inflated lung confirmed the excessive HA deposition in the distal lung parenchyma after IT bleomycin in TG mice as compared to injured WT mice (Fig. 4f).

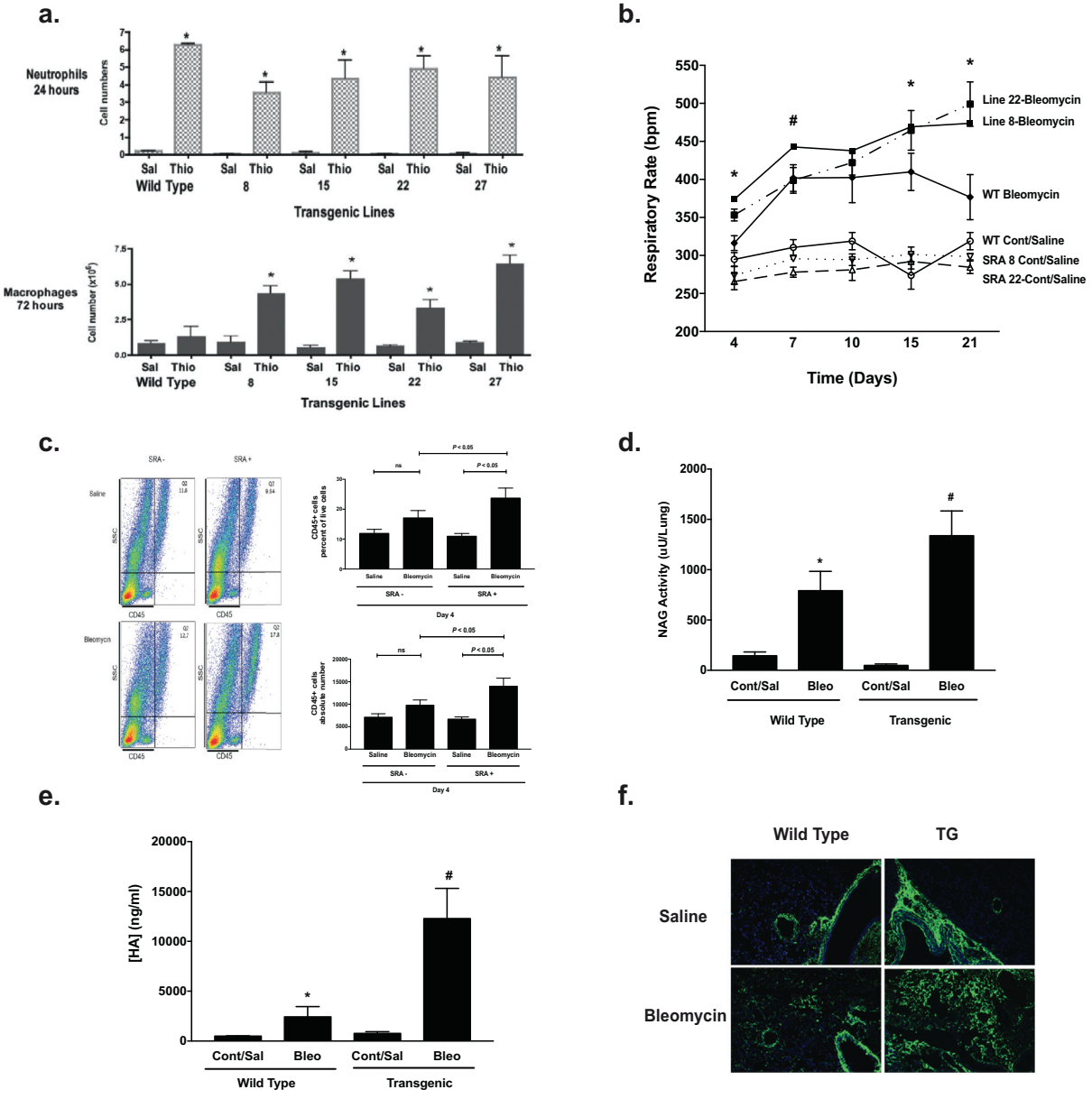

In order to determine the fibrotic changes due to IT bleomycin in WT and TG mice, we examined inflated fixed lungs using Masson's trichrome staining 21 days after IT treatments. WT mice given bleomycin had areas of cell infiltration and fibrosis, as well as areas of atelectasis (Fig. 5a). TG mice, on the other hand, showed extensive and intense fibrosis (Fig. 5a, data shown for SRA22). Fibrosis was quantified by Ashcroft score. WT mice injured with bleomycin had a six-fold increase in Ashcroft score (Fig. 5b). TG mice given bleomycin, however, had a 1.5-fold higher score than WT mice under the same injury conditions, suggesting an exaggerated fibrotic response (Fig. 5b). Fibrosis was quantified by determining the HPO content of the lung. WT mice showed a two-fold increase in lung HPO content after bleomycin injury (Fig. 5c). TG mice, on the other hand, had a further 25% increase in HPO content over WT bleomycin-injured mice (Fig. 5c).

Collectively, these data suggest that selective over-expression of RHAMM in macrophages is associated with a cell-specific activation of exaggerated inflammation and subsequent fibrosis, thereby establishing RHAMM as a critical determinant of the inflammatory and fibrotic outcomes of acute lung injury.

Discussion

We here report that mice with targeted deletion of RHAMM are protected from acute lung injury and fibrosis after IT bleomycin, with decreased weight loss, respiratory rates, inflammation and fibrosis. Transgenic mice with over-expression of RHAMM in macrophages are similar to WT mice at baseline. However, BMDM from transgenic mice had increased expression of the transgene on the cell surface, as well as increased chemotaxis to HA and endogenous proliferation. Of note, TG mice had exaggerated inflammatory and fibrotic responses when injured. In particular, TG mice had a macrophage-specific increased inflammatory response to chemically-induced peritonitis, and increased respiratory rates, lung inflammation and fibrosis after IT bleomycin. Collectively, these data suggest that RHAMM is a critical component of inflammation and fibrosis after injury and is a potential therapeutic target for anti-inflammatory and anti-fibrotic strategies.

Maximally increased HA occurs in conjunction with the early inflammatory response in a variety of human diseases and animal models. In particular, HA increases dramatically in the alveolar interstitium and BAL after intratracheal instillation of bleomycin in rodents [18,36–38,42]. Teder and coworkers showed that one of the principal mechanisms for this increase in HA is due to the elaboration of TGFβ1 [24]. This group also suggested that lower CD44 expression and decreased HA internalization as a result also contributes to an increased accumulation of HA [38]. Additionally, deletion of CD44 is associated with exaggerated inflammation with a failure to resolve inflammation after IT bleomycin [25]. However, Kasper et al. [23] have shown increased expression of CD44 and its variants after bleomycin injury. Our previous studies demonstrated increased RHAMM expression after bleomycin lung injury [31]. In those studies, inhibition of RHAMM using a blocking antibody decreased macrophage motility in vitro and limited the accumulation of macrophages in the lung after IT bleomycin [31]. Interestingly, therefore, the two major HA receptors have divergent effects on inflammation, one acting to promote inflammation (RHAMM), and the other acting to resolve inflammation (CD44) after acute lung injury.

Fig. 4. In vivo effects of transgenic overexpression of RHAMM in macrophages. (a). Intraperitoneal thioglycollate was used as a model of peritonitis. In all cases, IP saline did not elicit any inflammatory response. At 24 h after IP thioglycollate, WT and each TG mouse line showed equivalent accumulation of neutrophils in the peritoneal cavity. At 72 h, WT mice had no appreciable accumulation of macrophages in the peritoneal cavity. In contrast, each of the TG mouse lines had a 3–6-fold increase in macrophage infiltration in the peritoneal cavity in response to thioglycollate. (b). Respiratory rates after IT saline or bleomycin treatments showed that WT mice had a 30% increase in respiratory rate from days 7 to 14. TG mice (SRA8 and SRA22) showed a 30% increase in respiratory rate by 4 days after IT bleomycin and continued to worsen to almost 70% above baseline at 21 days. (c). Flow cytometry of lung cells on day 4 after IT treatments. At this early time point, SRA-WT control mice had no appreciable increase in CD45+ cells with bleomycin treatment measured both as percent of total cells and in absolute number. TG mice, however showed a two-fold increase in CD45+ cells with IT bleomycin ($P < 0.05$, data representative of two independent experiments). (d). Control mice had no increase in NAG activity as a measure of M1 macrophages. In WT mice given bleomycin, NAG activity of cells obtained by BAL was increased 4-fold ($^{*}P < 0.05$, n = 6–12). TG mice under the same conditions had a 7-fold increase in NAG activity ($^{\#}P < 0.01$ vs. WT bleomycin, n = 6–12). (e). HA content of BAL was determined on day 21. Control mice had no increases in lavage HA concentrations. In WT mice given bleomycin, the HA content of BAL increased 5-fold ($^{*}P < 0.01$, n = 6–12), whereas TG mice had a 20–25-fold increase in lavage HA content (# $P < 0.001$, n = 6–12). (f). Localization of HA in uninjured/control mice was around bronchiolar smooth muscle and in the adventitia of blood vessels. Bleomycin injury in WT mice was associated with a modest increase in distal lung HA staining. TG mice given IT bleomycin had substantially increased staining for HA in the lung parenchyma in concordance with the lavage HA content.

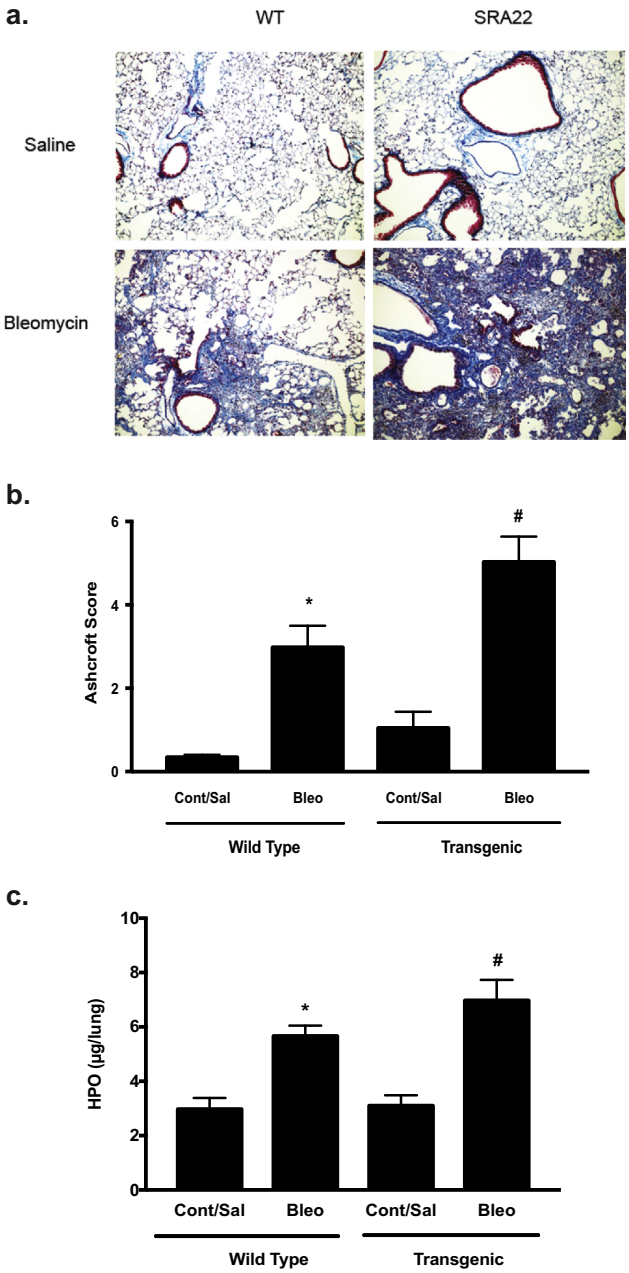

Fig. 5. Bleomycin-induced lung fibrosis in WT and RHAMM macrophage transgenic mice. (a). Trichrome staining of sections obtained from inflated and fixed WT and TG mice showed that control mice had normal lung architecture. IT bleomycin in WT mice was associated with patchy areas of cell infiltration and fibrosis, as well as atelectasis. TG mice injured with bleomycin had extensive and deeply blue staining indicative of worse fibrosis particularly around distal airways. Photomicrographs are all 100× magnification and representative of 6–12 animals. (b). Ashcroft score, used to quantify the degree of fibrosis, showed a 6-fold increase over controls in WT mice given bleomycin ($^{*}P < 0.01$, n = 6–12). TG mice given IT bleomycin had a 1.5-fold greater increase in Ashcroft score over that of WT mice with IT bleomycin ($^{\#}P < 0.05$, n = 6/group). (c). Hydroxyproline content was increased 2-fold over that of controls in WT mice injured with bleomycin ($^{*}P < 0.05$, n = 6 per group). Injured TG mice had a further 25% increase in HPO content over that of WT mice given bleomycin ($^{\#}P < 0.05$, n = 6/group).

Our previous studies in macrophages showed that an LPS/nucleic acid/protein-free 6-mer oligo HA (HA6) stimulated macrophage chemotaxis that could only be blocked by anti-RHAMM antibody and HA-binding peptide, but not three different antibodies to CD44, or antibodies to TLR2, TLR4 or TGFβ, suggesting that RHAMM is the receptor that mediates the effects of oligo-HA [43]. Effects on cell types other than inflammatory cells may also play a part in the observed effects of HA. Thus, overexpression of hyaluronan synthase 2 (*Has2*) in fibroblasts exaggerates bleomycin-induced lung fibrosis whereas fibroblast-specific deletion of *Has2* limits fibrosis [44], a process that may involve decreased senescence of fibroblasts to resolve fibrosis [45]. Additionally, deletion of *Has2* in alveolar type II cells, considered stem cells that are involved in lung repair after injury, is associated with increased fibrosis after bleomycin-induced lung injury [46]. It is likely that RHAMM also has cell-specific effects that influence the response to lung injury. Indeed, our studies show that the TG overexpression of RHAMM in macrophages was associated with exaggerated inflammation in both

the thioglycollate-induced peritonitis and IT bleomycin-induced lung injury models.

Activation of the innate immune system has been implicated in the regulation of inflammation and fibrosis in acute lung injury. Engagement of Toll-Like Receptors (TLRs) and co-receptors by endogenous danger-associated molecular patterns (DAMPs) activates the innate immune system [47–49]. This activation promotes the transcription of pro-IL1β and the formation of the NLRP3 inflammasome, a complex of three proteins (ASC, NLRP3 and pro-caspase1) that results in proteolytic activation of caspase-1, which in turn cleaves pro-IL1β to mature IL1β. The NLRP3 inflammasome promotes inflammation and fibrosis in a variety of lung diseases, including adult hyperoxia injury [50], IT bleomycin-induced lung injury [51] and the neonatal hyperoxia model of Bronchopulmonary Dysplasia (BPD) [34]. Indeed, low molecular weight (LMW) HA has been proposed as an endogenous DAMP [52–54]. Our previous studies showed that LMW HA can be derived from HMW HA via oxidative and nitrative stress, and that HA6 stimulates macrophage production of IL1β in vitro [55]. Thus, elaboration of cytokines and growth factors by recruited inflammatory cells likely drives excess HA production after bleomycin injury. We and others have also previously demonstrated that HA-binding peptides inhibit inflammation and fibrosis in the IT bleomycin model of injury [18], during skin wound repair [19], in ozone-induced airway hyper-responsiveness [21], and in the DNFB model of cutaneous inflammation [20]. It is possible that the effect of these peptides is to block the activation of the NLRP3 inflammasome, acting to prevent the initiation of inflammation, and thereby holding promise as therapeutic agents to limit the adverse effects of NLRP3 activation. This hypothesis is currently being studied.

Three different RHAMM KO mice, all on the C57/Bl6 background, have been developed to date. The mice used in the studies described here, developed by Tolg et al., disrupted the RHAMM gene between exons 8 and 16 and resulted in a truncated mRNA transcript, but no protein [56]. While these mice are viable and fertile, they have decreased fibroblast proliferation and, when crossed with APC mutant mice, show decreased desmoid tumors [56]. These mice also have a defect in fibroblast mitogenic signaling and delayed skin wound healing [57]. In addition, bone marrow-derived macrophages from these RHAMM KO mice fail to undergo chemotaxis to TGFβ1 and HA [43], and carotid artery ligation in these mice results in less constrictive remodeling of the artery and a wider arterial lumen [58]. Finally, our current studies show that these mice have decreased inflammation and fibrosis after bleomycin-induced acute lung injury. Li H et al. [59] disrupted exons 10 and 11 of RHAMM, generating a mouse that expresses a truncated RHAMM protein. These mice are also viable but showed defects in folliculogenesis and intact HA signaling to activate Erk [59]. Recently, Connell et al. have generated RHAMM knockout mice using ES cells from the European Conditional Mouse Mutagenesis Program that disrupted RHAMM exon 2 and generated mice that showed significant neonatal lethality, with defects in neural progenitor division and differentiation, and structural defects of the brain [60]. While it is likely that the differences observed in the mice described by Li et al. are due to the expression of a truncated protein, the differences between the Tolg and Connell mice, one viable without brain defects and the other with brain defects and neonatal death, are puzzling since neither one has RHAMM protein expression. It is possible that since the Connell mice were generated by high throughput mutagenesis, off target effects such as other genes or miRNA expression could also have been altered in those mice.

Several promoter constructs have been developed to drive myeloid-specific gene expression, including promoters for lysozyme, colony stimulating factor receptor and CD11c (reviewed in [61]). While expression of transgenes and reporter genes using these constructs demonstrate macrophage expression, strict specificity to macrophages is lacking. For example, LysM is also expressed in neutrophils and in alveolar type II cells. We used a construct consisting of gene elements regulating the transcription of macrophage Scavenger Receptor A (SRA) [62] to drive expression of a myc-tagged full length RHAMM cDNA in macrophages. SRA is a gene that is upregulated during monocyte to macrophage differentiation. The promoter construct consists of a 291 bp proximal promoter and a 400 bp upstream enhancer element that contain binding sites for critical transcription factors for macrophage differentiation [62]. In order to determine macrophage-specific effects of this promoter, we used the mouse thioglycollate-induced peritonitis model and demonstrated a macrophage-specific response that was exuberant and early in the TG mice, suggesting restricted expression of the transgene to macrophages. Despite these findings, given that most promoters lack specificity to macrophages, it would be prudent to be cautious in interpreting these data.

Of note, over-expression of RHAMM in macrophages resulted in exaggerated inflammation and fibrosis after IT bleomycin. These gain-of-function data compliment the observations in the RHAMM KO loss-of-function studies, and also strongly suggest cell-specific effects of RHAMM in regulating macrophage motility and proliferation. Given that the RHAMM macrophage over-expressing transgenic mice demonstrated exaggerated responses in both chemical peritonitis and acute lung injury models, they represent an excellent model system to be used in a wide variety of other inflammatory models and may be useful in the testing of anti-inflammatory

agents. Indeed, anti-RHAMM strategies hold significant therapeutic potential for the adverse consequences of lung injury in particular, but also for inflammatory disorders in general.

Methods

Reagents

Antibodies used in immunofluorescence assays and flow cytometry included F4/80 (Cat# ab6640, 10 μg/ml, Abcam, Cambridge, MA) to identify macrophages and anti-myc tag antibody (Cat# ab9106, 1:500 dilution, Abcam) to identify transgene expression. Murine CD44 was examined using the monoclonal antibody KM81 [63,64]. A rabbit polyclonal anti-RHAMM antibody, R36, was raised against amino acids 585–605 encoded in the full-length RHAMM cDNA [65] and purified to IgG fraction. Its specificity for RHAMM has been demonstrated previously [17]. A six-mer hyaluronan oligosaccharide (HA6, Cat# CSR-11007, Cosmobio, Tokyo, Japan) produced by enzymatic digestion of fermentation products of streptococcus sp. using mammalian hyaluronidase derived from ovine testis and purified by column chromatography. HA6 was demonstrated to be free of endotoxin, protein, and DNA, and the molecular size and purity were confirmed by fluorescence-assisted carbohydrate electrophoresis analysis and gas chromatography/mass spectroscopy (data not shown).

RHAMM KO mice and generation of transgenic mice with overexpression of RHAMM in macrophages

All animal procedures were carried out using protocols approved by the University of Texas Southwestern Medical Center, the University of Pennsylvania School of Medicine and the Children's Hospital of Philadelphia Institutional Animal Care and Utilization Committees in accordance with NIH guidelines. RHAMM knockout (KO) mice on a C57/Bl6 background have been reported previously [56], and were the kind gift of Dr. Eva A. Turley (Lawson Research Institute, London Regional Cancer Centre, London, Ontario, Canada). Littermate wild type (WT) mice generated during nine backcrosses with C57/Bl6J mice were used as controls.

We generated transgenic mice expressing human myc-tagged, full-length cDNA for mouse RHAMM (2.4 kb, mRHAMM) under the control of the macrophage-specific Scavenger Receptor A promoter, a kind gift of Dr. Steven Glass, (University of California, San Diego). First, full-length mouse RHAMM cDNA was introduced to the pCMV-Tag 3A plasmid using *EcoRI*/*XhoI* enzyme sites to generate human myc-tagged mRHAMM transgene. Next, the pCMV-Tag 3A mRHAMM plasmid was digested with *EcoRV*/*NotI* and introduced to the Scavenger Receptor A promoter-linked pAL.1 plasmid. Finally, the complete transgene construct of Scavenger Receptor A promoter linked to a human myc-tagged murine full-length wild type RHAMM cDNA was digested and sub-cloned to pBigT plasmid using *XhoI*/*NotI* enzyme sites (Fig. 3a). This construct was checked by both restriction enzyme digestion and sequencing. The pBigT-SRA-myc-mRHAMM plasmid was purified, linearized, and separated by agarose gel electrophoresis. Microinjection of DNA into C57/B6/J-129 mouse embryos was performed by the Transgenic Core at the University of Pennsylvania. Founder animals were screened by dot blot of tail genomic DNA and copy number was determined by dot blot comparison to a standard curve of the transgene (Supplementary Fig. 1). Transgenic lines were established from 4 founder animals, named SRA8, SRA15, SRA22 and SRA27. All had germline transmission of the transgene, which was maintained in heterozygote state. Littermates that were negative for the transgene were used as WT/SRA- controls for the experiments.

Intratracheal bleomycin model of acute lung injury and mouse lung harvest

Given the gender differences known in this model [32], only male mice were used for all bleomycin experiments. Animals were anesthetized with ketamine:xylazine (75:25 mg/kg), and the trachea was visualized through a vertical incision in the neck. Using an insulin syringe, 250 μl of either LPS-free saline or an equivalent volume of either 0.5 U/kg (WT or TG mice) or 1 U/kg (WT or RHAMM KO mice) bleomycin sulfate (Bristol Myers Squibb, Princeton, NJ) in saline was injected into the trachea. The incision was closed with surgical clips, and animals were harvested on either day 10, day 21 or day 28 after IT treatments. Bronchoalveolar lavage (BAL) was obtained (36 ml/kg, total lung capacity) and immediately centrifuged at 500 ×*g* for 10 min to pellet cells. Approximately 80–90% of lavage was routinely recovered. The cellular pellet and the supernatant were separated and frozen at −80 °C until further analysis. The pulmonary artery was perfused with PBS to remove all blood from the lungs. The left lung was inflated to 25 cm H_2O with 4% paraformaldehyde and placed in 10% neutral formalin for full fixation before processing for paraffin sectioning. The three lobes of the right lung were immediately frozen in liquid nitrogen and stored at −80 °C. Inflation fixed lungs were then processed to obtain 5 μm thick paraffin sections. For each time point, sections were stained with hematoxylin and eosin to examine lung architectural differences and by Masson's trichrome stain to identify fibrosis using light microscopy. Two independent and blinded observers scored at least five high power fields per

section from at least three sections per mouse to assess the severity of fibrosis, as described previously by Ashcroft [39].

Thioglycollate-induced model of peritonitis

The experimental approach to induce chemical peritonitis was performed as described by Baron and Proctor [66]. Three milliliters of calcium- and magnesium-free HBSS, pH 7.4, or thioglycollate broth (obtained from the Media Kitchen at the Wistar Institute, Philadelphia, PA) were injected intraperitoneally into each mouse. Either 24 or 72 h after intraperitoneal injection, the mice were euthanized by exposure to CO_2, and the abdominal cavities were lavaged with 5 ml of ice-cold HBSS to recover peritoneal cells. The volume recovered was noted, total cell concentration was determined with a Coulter counter (Hialeah, FL), and differential counts were performed on Wright-Giemsa-stained cytospin preparations.

Dual chamber plethysmography

Dual chamber plethysmography (Buxco Electronics Inc., Sharon, CT) was performed for non-invasive, non-sedated, real-time measurement of pulmonary function at various times after IT treatments. This airtight system, which separates the head from the body by a latex collar barrier, measures airflow across a pneumotach plate and uses a flow transducer to determine various parameters including respiratory rate (RR), which was used as a measure of respiratory distress.

Isolation of bone marrow-derived macrophages

BMDMs were obtained from respective WT, RHAMM KO and RHAMM macrophage over-expressing transgenic mice. Briefly, bone marrow was flushed from the tibia and femur of each mouse with macrophage medium (DMEM with 10% FCS, 20% L929 conditioned medium, 1% penicillin/streptomycin/glutamine) under sterile conditions. Marrow cells were made into a single-cell suspension by gentle pipetting and straining. Cells were centrifuged and resuspended, red blood cells were lysed by exposure to RBC lysis buffer, and then cells were cultured in macrophage medium. Non-adherent cells were replated and provided fresh medium. Cells were allowed to further differentiate for 3 days and were then used for assays.

ELISA-like assay for HA concentration

The concentration of HA in BAL was determined using a commercially available ELISA-like assay per manufacturer's instructions (Cat# K-1200, Echelon Biosciences Inc., Salt Lake City, UT).

N-Acetyl glucosaminidase (NAG) activity assay

The contents of macrophages in cell pellets obtained by BAL were measured by assaying NAG activity as previously described [34]. Briefly, the cell pellet from each mouse was lysed with 50 µl RIPA buffer (Sigma, St Louis, MO). For NAG activity, 20 µl of cell lysate or 25–400 µU of β-*N*-Acetyl Glucosaminidase standard (Sigma, St Louis, MO) was loaded in 96-well plates. Ten microliters of 0.1% TritonX and 20 µl of 15 mM *p*-nitrophenyl *N*-acetyl-β-D-glucosaminide (Sigma, St Louis, MO) were added to each well. After incubation at 37 °C for 30 min, 200 µl of 0.2 M sodium carbonate was added to each well to stop the reaction. The change in absorbance at 405 nm was measured as an index of NAG activity and correlates with macrophage content. Final results were obtained by multiplying NAG values by 2.5 to account for dilution during the assays.

Quantitative RT-PCR

Total RNA was extracted using RNeasy Plus Mini Kit (QIAGEN Inc., Valencia, CA), following manufacturer's instructions. Extracted RNA concentration of each sample was quantified using a NanoDrop ND-1000 Spectrophotometer (Thermo Fisher Scientific, Wilmington, DE). Reverse transcription was performed with 1 mg of total RNA in a 20 ml volume using iScript cDNA synthesis kit (Bio-Rad, Hercules, CA). The real-time quantitative PCR were performed on a 7900 HT fast real-time PCR system (Applied Biosystems, Foster, CA) using 2 ml cDNA, 7 ml diethylpyrocarbonate water, 10 ml SsoFast Probes Supermix with ROX (Bio-Rad, Hercules, CA) and 1 ml primer of TaqMan Gene Expression Assay. Forty cycles of amplification were performed. Cycle threshold (Ct) values were determined using SDS2.4 software. The gene of interest was normalized to the Ct value of the endogenous reference gene, 18 s rRNA, using the DCt method described by Pfaffl [67]. The following primer sets were used as supplied by Applied Biosystems: 18S: Mm03928990_g1, CD45: Mm01293577_m1, CD31: Mm01242576_m1, CD34: Mm00519283_m1, Fibronectin: Mm01256744_m1, CD105: Mm00468252_m1, and Collagen I: Mm00801666_g1. Transgene RNA analysis was accomplished using a primer set to amplify myc-RHAMM.

Western Blot

Western blot analysis was performed using the NOVEX NuPAGE electrophoresis system (Invitrogen, Grand Island, NY) with 1.5 mm 4–12% Bis–Tris gels according to manufacturer's instructions. Briefly, 25 mg of lung homogeneous was loaded to each well and gels were run at 100 V at 4 °C for 2 h in NuPAGE MOPS SDS running buffer under reducing conditions. Proteins were transferred to nitrocellulose

membrane at 80 V for 60 min at 4 °C. The membrane was then blocked for 1 h at room temperature with 5% BSA in Tween/Tris buffered saline (TTBS; 100 mM Tris base, 1.5 M NaCl adjusted to pH 7.4 with 0.1% Tween 20). Immunoblots were then incubated with myc-tag antibody overnight at 4 °C. The following day, the membrane was washed with TTBS three times, for 20 min each time. A horseradish peroxidase-conjugated goat anti-rabbit antibody (1:10,000, Santa Cruz Biotechnology, Santa Cruz, CA), used as the secondary antibody, was applied for 1 h at room temperature. Following this, the membrane was washed with TTBS followed by two 10-min washes with TBS. The blots were developed using a chemiluminescence system (Amersham Pharmacia Biotech, Piscataway, NJ).

Affinity histochemistry for HA

HA was localized using an avidin-biotin-FITC immunofluorescence technique as described with modifications [68]. Briefly, the sections were first treated with 1 M glycine to quench endogenous fluorescence. Then, sections were incubated overnight with the biotinylated HA binding region of aggrecan isolated from bovine nasal cartilage (bHABP, Cat# AMS.HKD-BC41, 1:250 dilution; AMS Biotechnology, Cambridge, MA). After washes, bHABP was detected using FITC-conjugated streptavidin (Sigma) and observed microscopically at a magnification of 100×. Specificity of staining for HA was confirmed both by incubation of the probe with excess HA before staining, and by pretreatment of the sections with *Streptomyces* hyaluronidase to degrade HA before staining (data not shown).

Hydroxyproline assay

Lung hydroxyproline (HPO) content was measured as an index of collagen content in whole mouse lungs according to methods previously described [69], with modifications. After perfusion of the lungs with PBS, they were removed, weighed and minced, and then hydrolyzed in 2 ml of 6 N HCl at 110 °C overnight. The resulting hydrolysate was neutralized with 2 ml of 6 N NaOH filtered through a 0.45-mm nylon membrane. One hundred microliters of this solution were then added to 1 ml of 1.4% chloramine T (Sigma, St. Louis, MO), 10% *n*-propanol, and 0.5 M sodium acetate, pH 6.0. After a 20-min incubation at room temperature, 1 ml of Ehrlich's reagent (1 M *p*-dimethylaminobenzaldehyde in 70% *n*-propanol and 20% perchloric acid) was added, and the resulting solution was incubated at 65 °C for 15 min. Absorbance was then measured at 550 nm, and the amount of HPO was determined against a standard curve produced with the use of known concentrations of HPO.

Isolation of lung cells and flow cytometry

Mice were sacrificed and perfused lungs were digested in RPMI medium containing collagenase XI (Sigma) and type IV bovine pancreatic DNase (Sigma) to obtain single-cell suspensions. After treatment with RBC lysis buffer, single-cell suspensions were surface stained with the following antibodies (eBioscience): CD45 (clone 30-F11), Ly6G (clone 1A8), F4/80 (clone BM8), CD4, CD11c (clone HL3) and CD86 (clone GL3). Flow cytometry was performed using BD FACS Canto cytometer (BD Bioscience) at the University of Texas Southwestern Flow Cytometry Core Facility, and data were analyzed with FlowJo software (TreeStar, Ashland, OR). For flow cytometry of BMDM, cells obtained from WT, KO and TG mice were cultured as described. Single cell suspensions were surface stained for myc, RHAMM and CD44 using normal IgG as a control. Flow cytometry was performed using BD FACS Canto cytometer (BD Bioscience) at the University of Texas Southwestern Flow Cytometry Core Facility.

Chemotaxis assay

Chemotaxis of BMDM was performed using a modified Boyden chemotaxis chamber containing a 96-well microchemotaxis plate (MBA-96; Neuro Probe, Cabin John, MD) as described previously with minor modifications [70]. Briefly, the bottom wells of the chamber contained 40 μl of HA6 (4 mM) dissolved in defined medium (DM), without FCS. Positive and negative controls included 10% FCS or DM, respectively. A 5-μm-pore polycarbonate membrane filter was placed between the bottom and top chamber. The upper wells were filled with 1×10^6 cells/ml suspended in 100 μl DM. The chamber was incubated for 6 h at 37 °C. Non-migratory cells on the upper surface of the membrane were treated with 200 μl of 1 mM EDTA for 15–20 min and wiped off. Cells that had migrated into the membrane were stained with Diff-Quick (Baxter Healthcare, McGaw Park, IL) and counted in five randomly selected high-power fields in each well. Each chemoattractant solution was tested in six wells and each experiment was repeated at least three times. Data were expressed as the number of macrophages that migrated into the membrane for each condition and converted to a percentage of control (DM) and data from three separate experiments were combined.

Statistical analysis

Group sample sizes of 6 in each group were predicted to achieve 95% power to detect a difference with a significance level (alpha) of 0.05 using a two-sided two-sample *t*-test. The investigators were blinded to group allocation during collection and analysis of

the data, and all inclusion/exclusion criteria were pre-established. Data are expressed as mean ± s.e.m. Normally distributed variables were analyzed by one factor analysis of variance (ANOVA) or unpaired Student's *t*-test. Non-parametric variables were compared using Mann–Whitney rank-sum tests. All statistical analyses were conducted using GraphPad Prism 7 software (GraphPad Software Inc., San Diego, CA). Significance for all statistical tests is shown in the figures and figure legends.

Supplementary data to this article can be found online at https://doi.org/10.1016/j.matbio.2018.08.002.

Acknowledgements

We would like to thank Dr. Eva Turley (Lawson Research Institute, London Regional Cancer Centre, London, Ontario, Canada) for the gift of the RHAMM KO mice and Dr. Christopher Glass (University of California, San Diego) for the gift of the SRA promoter plasmid used to generate transgenic mice.

Funding

The studies in this manuscript were funded by the NIH R01 awards HL62868, HL62472 and HL093535, and U01 award HL075900 to RCS, and R01 award HL079090 to HMD. Additional funding was obtained from the William Buchanan Chair in Pediatrics and Children's Hospital Foundation grant (#137) awarded to RCS.

Received 12 January 2018;
Received in revised form 9 July 2018;
Accepted 4 August 2018
Available online 8 August 2018

Keywords:
Acute lung injury;
Hyaluronan;
RHAMM;
Inflammation;
Fibrosis;
Knockout;
Transgenic mice

†These three authors contributed equally to the work presented in this manuscript.

References

[1] D.W. Shimabukuro, T. Sawa, M.A. Gropper, Injury and repair in lung and airways, Crit. Care Med. 31 (8 Suppl) (2003) S524–S531.
[2] L.B. Ware, M.A. Matthay, The acute respiratory distress syndrome, N. Engl. J. Med. 342 (18) (2000) 1334–1349.
[3] M. Selman, T.E. King Jr., A. Pardo, Idiopathic pulmonary fibrosis: prevailing and evolving hypotheses about its pathogenesis and implications for therapy, Ann. Intern. Med. 134 (2001) 136–151.
[4] C. Sharp, A.B. Millar, A.R. Medford, Advances in understanding of the pathogenesis of acute respiratory distress syndrome, Respiration 89 (5) (2015) 420–434.
[5] J. Hernnas, O. Nettelbladt, L. Bjermer, B. Sarnstrand, A. Malmstrom, R. Hällgren, Alveolar accumulation of fibronectin precedes fibrosis in bleomycin-induced pulmonary injury, Eur. Respir. J. 5 (4) (1992) 404–410.
[6] R. Raghow, S. Lurie, J.M. Seyer, A.H. Kang, Profiles of steady state levels of messenger RNAs coding for type I procollagen, elastin and fibronectin in hamster lungs undergoing bleomycin-induced interstitial pulmonary fibrosis, J. Clin. Invest. 76 (November) (1985) 1733–1739.
[7] A.J. Esposito, P.K. Bhatraju, R.D. Stapleton, M.M. Wurfel, C. Mikacenic, Hyaluronic acid is associated with organ dysfunction in acute respiratory distress syndrome, Crit. Care 21 (1) (2017) 304.
[8] T.C. Laurent, J.R.E. Fraser, Hyaluronan, FASEB J. 6 (1992) 2397–2404.
[9] A. Wang, C. de la Motte, M. Lauer, V. Hascall, Hyaluronan matrices in pathobiological processes, FEBS J. 278 (9) (2011) 1412–1418.
[10] R. Hällgren, A. Eklund, A. Engstrom-Laurent, B. Schmekel, Hyaluronate in bronchoalveolar lavage fluid: a new marker in sarcoidosis reflecting pulmonary disease, Br. Med. J. 290 (1985) 1778–1781.
[11] L. Bjermer, A. Engstrom-Laurent, R. Lundgren, L. Rosenhall, R. Hallgren, Hyaluronate and type III procollagen peptide concentrations in bronchoalveolar lavage fluid as markers of disease activity in farmer's lung, Br. Med. J. 295 (1987) 803–806.
[12] R. Hällgren, T. Samuelsson, T.C. Laurent, J. Modig, Accumulation of hyaluronan (hyaluronic acid) in the lung in adult respiratory distress syndrome, Am. Rev. Respir. Dis. 139 (1989) 682–687.
[13] T.N. Wight, C.W. Frevert, J.S. Debley, S.R. Reeves, W.C. Parks, S.F. Ziegler, Interplay of extracellular matrix and leukocytes in lung inflammation, Cell. Immunol. 312 (2017) 1–14.
[14] H.C. DeGrendele, P. Estess, L.J. Picker, M.H. Siegelman, CD44 and its ligand hyaluronate mediate rolling under physiologic flow: a novel lymphocyte-endothelial cell primary adhesive pathway, J. Exp. Med. 183 (3) (1996) 1119–1130.
[15] M. Mohamadzadeh, H. DeGrendele, H. Arizpe, P. Estess, M. Siegelman, Proinflammatory stimuli regulate endothelial hyaluronan expression and CD44/HA-dependent primary adhesion, J. Clin. Invest. 101 (1) (1998) 97–108.
[16] M.H. Siegelman, H.C. DeGrendele, P. Estess, Activation and interaction of CD44 and hyaluronan in immunological systems, J. Leukoc. Biol. 66 (2) (1999) 315–321.
[17] R.C. Savani, C. Wang, B. Yang, S. Zhang, M.G. Kinsella, T.N. Wight, R. Stern, D.M. Nance, E.A. Turley, Migration of bovine aortic smooth muscle cells after wounding injury. The role of hyaluronan and RHAMM, J. Clin. Invest. 95 (3) (1995) 1158–1168.
[18] R.C. Savani, G. Hou, P. Liu, C. Wang, E. Simons, P.C. Grimm, R. Stern, A.H. Greenberg, H.M. DeLisser, N. Khalil, A role for hyaluronan in macrophage accumulation and collagen deposition after bleomycin-induced lung injury, Am. J. Respir. Cell Mol. Biol. 23 (4) (2000) 475–484.

[19] C. Tolg, S.R. Hamilton, E. Zalinska, L. McCulloch, R. Amin, N. Akentieva, F. Winnik, R. Savani, D.J. Bagli, L.G. Luyt, M.K. Cowman, J.B. McCarthy, E.A. Turley, A RHAMM mimetic peptide blocks hyaluronan signaling and reduces inflammation and fibrogenesis in excisional skin wounds, Am. J. Pathol. 181 (4) (2012) 1250–1270.
[20] M.E. Mummert, M. Mohamadzadeh, D.I. Mummert, N. Mizumoto, A. Takashima, Development of a peptide inhibitor of hyaluronan-mediated leukocyte trafficking, J. Exp. Med. 192 (6) (2000) 769–779.
[21] S. Garantziotis, Z. Li, E.N. Potts, K. Kimata, L. Zhuo, D.L. Morgan, R.C. Savani, P.W. Noble, W.M. Foster, D.A. Schwartz, J.W. Hollingsworth, Hyaluronan mediates ozone-induced airway hyperresponsiveness in mice, J. Biol. Chem. 284 (17) (2009) 11309–11317.
[22] R.C. Savani, H.M. DeLisser, Hyaluronan and its receptors in lung health and disease, in: H.G. Garg, P.J. Roughley, C.A. Hales (Eds.), Proteoglycans and Lung Disease, Marcel Dekker, New York 2003, pp. 73–106.
[23] M. Kasper, A. Bierhaus, A. Whyte, R.M. Binns, D. Schuh, M. Muller, Expression of CD44 isoforms during bleomycin- or radiation-induced pulmonary fibrosis in rats and mini-pigs, Histochem. Cell Biol. 105 (1996) 221–230.
[24] P. Teder, O. Nettelbladt, P. Heldin, Characterization of the mechanism involved in bleomycin-induced increased hyaluronan production in rat lung, Am. J. Respir. Cell Mol. Biol. 12 (1995) 181–189.
[25] P. Teder, R.W. Vandivier, D. Jiang, J. Liang, L. Cohn, E. Pure, P.M. Henson, P.W. Noble, Resolution of lung inflammation by CD44, Science 296 (5565) (2002) 155–158.
[26] C. Hardwick, K. Hoare, R. Owens, H.P. Hohn, M. Hook, D. Moore, V. Cripps, L. Austen, D.M. Nance, E.A. Turley, Molecular cloning of a novel hyaluronan receptor that mediates tumor cell motility, J. Cell Biol. 117 (6) (1992) 1343–1350.
[27] C.L. Hall, B. Yang, X. Yang, S. Zhang, M. Turley, S. Samuel, L.A. Lange, C. Wang, G.D. Curpen, R.C. Savani, A.H. Greenberg, E.A. Turley, Overexpression of the hyaluronan receptor RHAMM is transforming and is also required for H-ras transformation, Cell 82 (1) (1995) 19–26.
[28] D. Jiang, J. Liang, P.W. Noble, Hyaluronan as an immune regulator in human diseases, Physiol. Rev. 91 (1) (2011) 221–264.
[29] C.L. Hall, L.A. Collis, A.J. Bo, L. Lange, A. McNicol, J.M. Gerrard, E.A. Turley, Fibroblasts require protein kinase C activation to respond to hyaluronan with increased locomotion, Matrix Biol. 20 (3) (2001) 183–192.
[30] D. Manzanares, M.E. Monzon, R.C. Savani, M. Salathe, Apical oxidative hyaluronan degradation stimulates airway ciliary beating via RHAMM and RON, Am. J. Respir. Cell Mol. Biol. 37 (2) (2007) 160–168.
[31] A. Zaman, Z. Cui, J.P. Foley, H. Zhao, P.C. Grimm, H.M. Delisser, R.C. Savani, Expression and role of the hyaluronan receptor RHAMM in inflammation after bleomycin injury, Am. J. Respir. Cell Mol. Biol. 33 (5) (2005) 447–454.
[32] J.W. Voltz, J.W. Card, M.A. Carey, L.M. Degraff, C.D. Ferguson, G.P. Flake, J.C. Bonner, K.S. Korach, D.C. Zeldin, Male sex hormones exacerbate lung function impairment after bleomycin-induced pulmonary fibrosis, Am. J. Respir. Cell Mol. Biol. 39 (1) (2008) 45–52.
[33] R.C. Savani, R.I. Godinez, M.H. Godinez, E. Wentz, A. Zaman, Z. Cui, P.M. Pooler, S.H. Guttentag, M.F. Beers, L.W. Gonzales, P.L. Ballard, Respiratory distress after intratracheal bleomycin: selective deficiency of surfactant proteins B and C, Am. J. Phys. Lung Cell. Mol. Phys. 281 (2001) L685–L696.
[34] J. Liao, V.S. Kapadia, L.S. Brown, N. Cheong, C. Longoria, D. Mija, M. Ramgopal, J. Mirpuri, D.C. McCurnin, R.C. Savani, The NLRP3 inflammasome is critically involved in the development of bronchopulmonary dysplasia, Nat. Commun. 6 (2015) 8977.
[35] T. Nitta, K. Okumura, K. Sato, Lysosomal enzymic activity in astroglial cells, Pathobiology 60 (1) (1992) 42–44.
[36] B.A. Bray, P.M. Sampson, M. Osman, A. Giandomenico, G.M. Turino, Early changes in lung tissue hyaluronan (hyaluronic acid) and hyaluronidase in bleomycin-induced alveolitis in hamsters, Am. Rev. Respir. Dis. 143 (1991) 284–288.
[37] O. Nettelbladt, R. Hallgren, Hyaluronan (hyaluronic acid) in bronchoalveolar fluid during the development of bleomycin-induced alveolitis in the rat, Am. Rev. Respir. Dis. 140 (1989) 1028–1032.
[38] P. Teder, P. Heldin, Mechanism of impaired local hyaluronan turnover in bleomycin-induced lung injury in rat, Am. J. Respir. Cell Mol. Biol. 17 (3) (1997) 376–385.
[39] T. Ashcroft, J.M. Simpson, V. Timbrell, Simple method of estimating severity of pulmonary fibrosis on a numerical scale, J. Clin. Pathol. 41 (4) (1988) 467–470.
[40] S. Mattoli, A. Bellini, M. Schmidt, The role of a human hematopoietic mesenchymal progenitor in wound healing and fibrotic diseases and implications for therapy, Curr. Stem. Cell Res. Ther. 4 (4) (2009) 266–280.
[41] J. Chan, P.J. Leenen, I. Bertoncello, S.I. Nishikawa, J.A. Hamilton, Macrophage lineage cells in inflammation: characterization by colony-stimulating factor-1 (CSF-1) receptor (c-Fms), ER-MP58, and ER-MP20 (Ly-6C) expression, Blood 92 (4) (1998) 1423–1431.
[42] O. Nettelbladt, J. Bergh, M. Schenholm, A. Tengblad, R. Hallgren, Accumulation of hyaluronic acid in the alveolar interstitial tissue in bleomycin-induced alveolitis, Am. Rev. Respir. Dis. 139 (1989) 759–762.
[43] J.P. Foley, D. Lam, H. Jiang, J. Liao, N. Cheong, T.M. McDevitt, A. Zaman, J.R. Wright, R.C. Savani, Toll-like receptor 2 (TLR2), transforming growth factor-beta, hyaluronan (HA), and receptor for HA-mediated motility (RHAMM) are required for surfactant protein A-stimulated macrophage chemotaxis, J. Biol. Chem. 287 (44) (2012) 37406–37419.
[44] Y. Li, D. Jiang, J. Liang, E.B. Meltzer, A. Gray, R. Miura, L. Wogensen, Y. Yamaguchi, P.W. Noble, Severe lung fibrosis requires an invasive fibroblast phenotype regulated by hyaluronan and CD44, J. Exp. Med. 208 (7) (2011) 1459–1471.
[45] Y. Li, J. Liang, T. Yang, J. Monterrosa Mena, C. Huan, T. Xie, A. Kurkciyan, N. Liu, D. Jiang, P.W. Noble, Hyaluronan synthase 2 regulates fibroblast senescence in pulmonary fibrosis, Matrix Biol. 55 (2016) 35–48.
[46] J. Liang, Y. Zhang, T. Xie, N. Liu, H. Chen, Y. Geng, A. Kurkciyan, J.M. Mena, B.R. Stripp, D. Jiang, P.W. Noble, Hyaluronan and TLR4 promote surfactant-protein-C-positive alveolar progenitor cell renewal and prevent severe pulmonary fibrosis in mice, Nat. Med. 22 (11) (2016) 1285–1293.
[47] L. Broderick, D. De Nardo, B.S. Franklin, H.M. Hoffman, E. Latz, The inflammasomes and autoinflammatory syndromes, Annu. Rev. Pathol. 10 (2015) 395–424.
[48] M. Lamkanfi, T.D. Kanneganti, Nlrp3: an immune sensor of cellular stress and infection, Int. J. Biochem. Cell Biol. 42 (6) (2010) 792–795.
[49] F.S. Sutterwala, S. Haasken, S.L. Cassel, Mechanism of NLRP3 inflammasome activation, Ann. N. Y. Acad. Sci. 1319 (2014) 82–95.
[50] J. Fukumoto, I. Fukumoto, P.T. Parthasarathy, R. Cox, B. Huynh, G.K. Ramanathan, R.B. Venugopal, D.S. Allen-

Gipson, R.F. Lockey, N. Kolliputi, NLRP3 deletion protects from hyperoxia-induced acute lung injury, Am. J. Phys. Cell Physiol. 305 (2) (2013) C182–C189.
[51] P. Gasse, C. Mary, I. Guenon, N. Noulin, S. Charron, S. Schnyder-Candrian, B. Schnyder, S. Akira, V.F. Quesniaux, V. Lagente, B. Ryffel, I. Couillin, IL-1R1/MyD88 signaling and the inflammasome are essential in pulmonary inflammation and fibrosis in mice, J. Clin. Invest. 117 (12) (2007) 3786–3799.
[52] K.R. Taylor, R.L. Gallo, Glycosaminoglycans and their proteoglycans: host-associated molecular patterns for initiation and modulation of inflammation, FASEB J. 20 (1) (2006) 9–22.
[53] K.R. Taylor, K. Yamasaki, K.A. Radek, A. Di Nardo, H. Goodarzi, D. Golenbock, B. Beutler, R.L. Gallo, Recognition of hyaluronan released in sterile injury involves a unique receptor complex dependent on Toll-like receptor 4, CD44, and MD-2, J. Biol. Chem. 282 (25) (2007) 18265–18275.
[54] K. Yamasaki, J. Muto, K.R. Taylor, A.L. Cogen, D. Audish, J. Bertin, E.P. Grant, A.J. Coyle, A. Misaghi, H.M. Hoffman, R.L. Gallo, NLRP3/cryopyrin is necessary for Interleukin-1{beta} (IL-1{beta}) release in response to hyaluronan, an endogenous trigger of inflammation in response to injury, J. Biol. Chem. 284 (19) (2009) 12762–12771.
[55] H.C. Østerholt, I. Dannevig, M.H. Wyckoff, J. Liao, Y. Akgul, M. Ramgopal, D.S. Mija, N. Cheong, C. Longoria, M. Mahendroo, B. Nakstad, O.D. Saugstad, R.C. Savani, Antioxidant protects against increases in low molecular weight hyaluronan and inflammation in asphyxiated newborn pigs resuscitated with 100% oxygen, PLoS One 7 (6) (2012), e38839.
[56] C. Tolg, R. Poon, R. Fodde, E.A. Turley, B.A. Alman, Genetic deletion of receptor for hyaluronan-mediated motility (Rhamm) attenuates the formation of aggressive fibromatosis (desmoid tumor), Oncogene 22 (44) (2003) 6873–6882.
[57] C. Tolg, S.R. Hamilton, K.-A. Nakrieko, F. Kooshesh, P. Walton, J.B. McCarthy, M.J. Bissell, E.A. Turley, RHAMM–/– fibroblasts are defective in CD44-mediated ERK1/2 mitogenic signaling leading to defective skin wound repair, J. Cell Biol. 175 (6) (2007) 1017–1028.
[58] X. Ma, J.D. Pearce, D.B. Wilson, W.P. English, M.S. Edwards, R.L. Geary, Loss of the hyaluronan receptor RHAMM prevents constrictive artery wall remodeling, J. Vasc. Surg. 59 (3) (2014) 804–813.
[59] H. Li, J. Moll, A. Winkler, L. Frappart, S. Brunet, J. Hamann, T. Kroll, M.H. Verlhac, H. Heuer, P. Herrlich, A. Ploubidou, RHAMM deficiency disrupts folliculogenesis resulting in female hypofertility, Biol. Open 4 (4) (2015) 562–571.
[60] M. Connell, H. Chen, J. Jiang, C.W. Kuan, A. Fotovati, T.L. Chu, Z. He, T.C. Lengyell, H. Li, T. Kroll, A.M. Li, D. Goldowitz, L. Frappart, A. Ploubidou, M.S. Patel, L.M. Pilarski, E.M. Simpson, P.F. Lange, D.W. Allan, C.A. Maxwell, HMMR acts in the PLK1-dependent spindle positioning pathway and supports neural development, elife 6 (2017).
[61] D.A. Hume, Applications of myeloid-specific promoters in transgenic mice support in vivo imaging and functional genomics but do not support the concept of distinct macrophage and dendritic cell lineages or roles in immunity, J. Leukoc. Biol. 89 (4) (2011) 525–538.
[62] A. Horvai, W. Palinski, H. Wu, K.S. Moulton, K. Kalla, C.K. Glass, Scavenger receptor A gene regulatory elements target gene expression to macrophages and to foam cells of atherosclerotic lesions, Proc. Natl. Acad. Sci. U. S. A. 92 (12) (1995) 5391–5395.
[63] K. Miyake, K.L. Medina, S.-I. Hayashi, S. Ono, T. Hamaoka, P.W. Kincade, Monoclonal antibodies to Pgp-1/CD44 block lympho-hemopoiesis in long-term bone marrow cultures, J. Exp. Med. 171 (February) (1990) 477–488.
[64] K. Miyake, C.B. Underhill, J. Lesley, P.W. Kincade, Hyaluronate can function as a cell adhesion molecule and CD44 participates in hyluronate recognition, J. Exp. Med. 172 (1) (1990) 69–75.
[65] C. Fieber, R. Plug, J. Sleeman, P. Dall, H. Ponta, M. Hofmann, Characterization of the murine gene encoding the intracellular hyaluronan receptor IHABP (RHAMM), Gene 226 (1) (1999) 41–50.
[66] E.J. Baron, R.A. Proctor, Elicitation of peritoneal polymorphonuclear neutrophils from mice, J. Immunol. Methods 49 (3) (1982) 305–313.
[67] M.W. Pfaffl, A new mathematical model for relative quantification in real-time RT-PCR, Nucleic Acids Res. 29 (9) (2001), e45.
[68] J.A. Ripellino, M.M. Killinger, R.U. Margolis, R.K. Margolis, The hyaluronic acid binding region as a specific probe for the localization of hyaluronic acid in tissue sections, J. Hisotchem. Cytochem. 33 (1985) 1066–1086.
[69] J.F. Woessner Jr., The determination of hydroxyproline in tissue and protein samples containing small proportions of this imino acid, Arch. Biochem. Biophys. 93 (1961) 440–447.
[70] Y. Shi, B.S. Kornovski, R.C. Savani, E.A. Turley, A rapid, multiwell colorometric assay for chemotaxis, J. Immunol. Methods 164 (1993) 149–154.